Spectrochimica Acta Part A 85 (2012) 179–189

Contents lists available at SciVerse ScienceDirect

Spectrochimica Acta Part A: Molecular and Biomolecular Spectroscopy

journal homepage: www.elsevier.com/locate/saa

FT-IR, FT-Raman, NMR and UV–vis spectra, vibrational assignments and DFT calculations of 4-butyl benzoic acid

M. Karabacak[a], Z. Cinar[a], M. Kurt[b], S. Sudha[c], N. Sundaraganesan[c,*]

[a] Department of Physics, Afyon Kocatepe University, 03040 Afyonkarahisar, Turkey
[b] Department of Physics, Ahi Evran University, 40100 Kırşehir, Turkey
[c] Department of Physics (Engg.), Annamalai University, Annamalai Nagar, Chidambaram 608002, Tamil Nadu, India

ARTICLE INFO

Article history:
Received 26 August 2011
Received in revised form
24 September 2011
Accepted 27 September 2011

Keywords:
DFT
Vibrational spectra
NMR
UV–vis spectra
4-Butyl benzoic acid
Dimer

ABSTRACT

The solid phase FTIR and FT-Raman spectra of 4-butyl benzoic acid (4-BBA) have been recorded in the regions 400–4000 and 50–4000 cm^{-1}, respectively. The spectra were interpreted in terms of fundamentals modes, combination and overtone bands. The structure of the molecule was optimized and the structural characteristics were determined by density functional theory (DFT) using B3LYP method with 6-311++G(d,p) as basis set. The vibrational frequencies were calculated for monomer and dimer by DFT method and were compared with the experimental frequencies, which yield good agreement between observed and calculated frequencies. The infrared and Raman spectra were also predicted from the calculated intensities. ^{13}C and ^{1}H NMR spectra were recorded and ^{13}C and ^{1}H nuclear magnetic resonance chemical shifts of the molecule were calculated using the gauge independent atomic orbital (GIAO) method. UV–visible spectrum of the compound was recorded in the region 200–400 nm and the electronic properties HOMO and LUMO energies were measured by time-dependent TD-DFT approach. The geometric parameters, energies, harmonic vibrational frequencies, IR intensities, Raman intensities, chemical shifts and absorption wavelengths were compared with the available experimental data of the molecule.

1. Introduction

Benzoic acid is widely found in plants and animals and is used in miticides, as contrast media in urology, for cholecystrographic examination and in the manufacture of pharmaceuticals. Benzoic acids and their salts are permitted food preservatives in many types of foods [1]. Benzoic acid inhibits bacterial development. Although these preservatives prevent or delay nutritional losses due to microbiological, enzymatic or chemical changes of foods during its shelf life, they are harmful at higher than permitted safety levels. Therefore, their determination is a mandatory step in routine food analyses. Benzoic acid derivatives are used in medicine as a protective drug against UV radiation in the diagnosis of gastrointestinal disorders and therapeutically in fibrotic skin disorders [2]. Substituted benzoic acids are very important materials in chemical and pharmaceutical industries and can be prepared by oxidation of the corresponding substituted toluenes [3–5]. A recent patent reported that, their activity being related to novel synergistic compositions that selectively control tumor tissue [6].

Until now, the experimental and theoretical investigation of benzoic acid molecule with various substitutions except butyl group has been made [7–13]. In these works, the geometrical parameters and vibrational frequencies were calculated and were compared with the experimental results. To our knowledge, no attempts to theoretically assign the experimental vibrational spectra of 4-butyl benzoic acid (4-BBA) have been done yet.

In the present work, in addition the above results, the first order hyperpolarizability, NMR analysis and UV spectral analysis of 4-BBA have been investigated. The theoretically predicted values have been compared with the experimentally measured data and also the results have been discussed. Theoretical studies of pharmaceutical compounds are of interest in order to gain a deeper approaching on their action and thus helping in the design of new compounds with therapeutic effects. Now-a-days, the progress of various theoretical methods has made possible the calculation of vibrational potential fields of medium size molecules with moderate computational effort. Organic molecules able to manipulate photonic signals efficiently are of importance in technologies such as optical communication, optical computing, and dynamic image processing [14,15]. The knowledge of physico-chemical properties and sites of reaction of title compound will provide a deeper insight of its probable action.

* Corresponding author. Tel.: +91 9442068405.
E-mail address: sundaraganesan_n2003@yahoo.co.in (N. Sundaraganesan).

1386-1425/$ – see front matter © 2011 Elsevier B.V. All rights reserved.
doi:10.1016/j.saa.2011.09.058

2. Experimental

The 4-butyl benzoic acid (4-BBA) sample was purchased from Sigma-Aldrich Company with a stated purity 97% and it was used as such without further purification. The FTIR spectrum of molecule was recorded in the region 400–4000 cm^{-1} on a Perkin Elmer FTIR BX spectrometer calibrated using polystyrene bands. The sample was prepared using a KBr disc technique because of solid state. The FT-Raman spectrum was recorded using 1064 nm line of Nd:YAG laser as excitation wave length in the region 50–4000 cm^{-1} on a Bruker RFS 100/S FT-Raman. The detector is a liquid nitrogen cooled Ge detector. Five hundred scans were accumulated at 4 cm^{-1} resolution using a laser power of 100 mW. The UV–vis absorption spectrum of the compound was recorded in ethanol and water solution using a Shimadzu 1800 PC spectrophotometer in the spectral region of 200–400 nm. NMR experiments were performed in Bruker DPX 600 MHz at 300 K. The compound was dissolved in DMSO, and chemical shifts were reported in ppm relative to tetramethylsilane (TMS).

3. Computational details

The molecular geometry is directly taken from the X-ray diffraction experimental results without any constraints. In the next step, the DFT calculations with a hybrid functional B3LYP (Becke's three parameter hybrid functional using the LYP correlation functional) at 6-311++G(d,p) basis set were performed with the Gaussian 03W software package [16] and Gauss view visualization program [17]. The total energy distribution (TED) corresponding to each of the observed frequencies is calculated using VEDA 4 program [18] and it shows the reliability and accuracy of the spectral analysis. The isotropic chemical shifts are frequently used as an aid in identification of organic compounds and accurate predictions of molecular geometries are essential for reliable studies of magnetic properties. The B3LYP method allows calculating the shielding constants with accuracy and the GIAO method is one of the most common approaches for calculating nuclear magnetic shielding tensors. The ^{13}C and ^{1}H NMR isotropic shielding were calculated with the GIAO method [19,20] using the optimized parameters obtained from B3LYP/6-311++G(d,p) method. UV–vis spectra, electronic transitions, vertical excitation energies, absorbance and oscillator strengths were computed with the time-dependent DFT method. The electronic properties such as HOMO and LUMO energies were determined by time-dependent DFT (TD-DFT) approach.

4. Prediction of Raman intensities and first order hyperpolarizability

The Raman activities (S_{Ra}) calculated with Gaussian 03 program [16] converted to relative Raman intensities (I_{Ra}) using the following relationship derived from the intensity theory of Raman scattering [21,22],

$$I_i = \frac{f(\nu_0 - \nu_i)^4 S_i}{\nu_i[1 - \exp(-hc\nu_i/kT)]}$$

where ν_0 is the laser exciting wavenumber in cm^{-1} (in this work, we have used the excitation wavenumber ν_0 = 9398.5 cm^{-1}, which corresponds to the wavelength of 1064 nm of a Nd:YAG laser), ν_i the vibrational wavenumber of the ith normal mode (cm^{-1}), while S_i is the Raman scattering activity of the normal mode ν_i. f (is a constant equal to 10^{-12}) is a suitably chosen common normalization factor for all peak intensities. h, k, c and T are Planck and Boltzmann constants, speed of light and temperature in Kelvin, respectively.

The first hyperpolarizability (β_0) of this novel molecular system, and related properties (β, α_0 and $\Delta\alpha$) of 4-BBA are calculated using B3LYP/6-311++G(d,p) method, based on the finite-field approach. In the presence of an applied electric field, the energy of a system is a function of the electric field. First order hyperpolarizability is a third rank tensor that can be described by 3 × 3 × 3 matrices. The 27 components of the 3D matrix can be reduced to 10 components due to the Kleinman symmetry [23]. It can be given in the lower tetrahedral format. It is obvious that the lower part of the 3 × 3 × 3 matrices is a tetrahedral. The components of β are defined as the coefficients in the Taylor series expansion of the energy in the external electric field. When the external electric field is weak and homogeneous, this expansion becomes:

$$E = E^0 - \mu_\alpha F_\alpha - \frac{1}{2\alpha_{\alpha\beta}F_\alpha F_\beta} - \frac{1}{6\beta_{\alpha\beta\gamma}F_\alpha F_\beta F_\gamma} + \cdots$$

where E^0 is the energy of the unperturbed molecules, F_α is the field at the origin, μ_α, $\alpha_{\alpha\beta}$ and $\beta_{\alpha\beta\gamma}$ are the components of dipole moment, polarizability and the first order hyperpolarizabilities, respectively. The total static dipole moment μ, the mean polarizability α_0, the anisotropy of the polarizability $\Delta\alpha$ and the mean first order hyperpolarizability β_0, using the x, y, z components they are defined as:

$$\mu = (\mu_x^2 + \mu_y^2 + \mu_z^2)^{1/2}$$
$$\alpha_0 = \frac{\alpha_{xx} + \alpha_{yy} + \alpha_{zz}}{3}$$
$$\alpha = 2^{-1/2}[(\alpha_{xx} - \alpha_{yy})^2 + (\alpha_{yy} - \alpha_{zz})^2 + (\alpha_{zz} - \alpha_{xx})^2 + 6\alpha^2 XX]^{1/2}$$
$$\beta_0 = (\beta_x^2 + \beta_y^2 + \beta_z^2)^{1/2}$$

and

$$\beta_x = \beta_{xxx} + \beta_{xyy} + \beta_{xzz}$$
$$\beta_y = \beta_{yyy} + \beta_{xxy} + \beta_{yzz}$$
$$\beta_z = \beta_{zzz} + \beta_{xxz} + \beta_{yyz}$$

Since the values of the polarizabilities (α) and hyperpolarizability (β) of the Gaussian 03 output are reported in atomic units (a.u.), the calculated values have been converted into electrostatic units (esu) (α: 1 a.u. = 0.1482 × 10^{-24} esu; β: 1 a.u. = 8.639 × 10^{-33} esu).

The total molecular dipole moment and first order hyperpolarizability are 2.7983 dB and 5.9017 × 10^{-30} esu, respectively and are depicted in Table 1. Total dipole moment of title molecule is approximately two times greater than those of urea and first order hyperpolarizability of title molecule is 15 times greater than those of urea (μ and β of urea are 1.3732 dB and 0.3728 × 10^{-30} esu obtained by HF/6-311G(d,p) method).

Table 1
The electric dipole moment (D), polarizability and first hyperpolarizability of 4-BBA.

	a.u.	esu (×10^{-24})		a.u.	esu (×10^{-33})
α_{xx}	169.4434	25.1115	β_{xxx}	329.0050	2842.3728
α_{xy}	−5.5459	−0.8219	β_{xxy}	75.8083	654.9310
α_{yy}	111.8403	16.5747	β_{xyy}	−31.2834	−270.2666
α_{xz}	−39.5145	−5.8560	β_{yyy}	−11.3476	−98.0353
α_{yz}	−17.9434	−2.6592	β_{xxz}	−337.7997	−2918.3525
α_{zz}	141.6800	20.9970	β_{xyz}	−33.3823	−288.3999
α_{tot}	140.9879	20.8944	β_{yyz}	33.7733	291.7779
$\Delta\alpha$	199.8076	29.6115	β_{xzz}	228.6767	1975.6064
μ_x	−2.6488		β_{yzz}	−4.6850	−40.4751
μ_y	0.6170		β_{zzz}	−127.2310	−1099.1870
μ_z	0.6586		β_{tot}	683.1187	5901.6676
μ	2.7983				

5. Results and discussion

5.1. Structural analysis

The optimized structural parameters bond length and bond angle for the thermodynamically preferred geometry of 4-BBA

Table 2
Comparison of the geometrical parameters of 4-BBA, bond lengths in angstrom, angles in degrees.

Bond lengths (Å)	X-ray	Monomer	Dimer	Bond angles (°)	X-ray	Monomer	Dimer
C(1)–C(2)	1.36[a]	1.40	1.40	C(2)–C(1)–C(6)	123[a]	121.5	121.4
C(1)–C(6)	1.42[a]	1.39	1.39	C(1)–C(2)–C(3)	118[a]	118.0	118.0
C(2)–C(3)	1.37[a]	1.40	1.40	C(1)–C(2)–C(14)		118.9	118.9
C(2)–C(14)		1.52	1.52	C(3)–C(2)–C(14)		123.2	123.1
C(3)–C(4)	1.41[a]	1.39	1.39	C(2)–C(3)–C(4)	122[a]	121.0	121.0
C(4)–C(5)	1.39[a]	1.40	1.40	C(3)–C(4)–C(5)	120[a]	120.4	120.4
C(5)–C(6)	1.39[a]	1.40	1.40	C(4)–C(5)–C(6)	119[a]	119.2	119.2
C(5)–C(9)		1.48	1.48	C(4)–C(5)–C(9)	119[a]	118.4	119.1
C(14)–C(15)	1.52[a]	1.53	1.53	C(6)–C(5)–C(9)	122[a]	122.4	121.7
C(15)–C(16)	1.51[a]	1.53	1.53	C(1)–C(6)–C(5)	118[a]	119.9	120.0
C(16)–C(17)	1.52[a]	1.53	1.53	C(2)–C(14)–C(15)		117.2	117.1
C(9)–O(10)	1.29[a]	1.36	1.32	C(14)–C(15)–C(16)		112.6	112.7
C(9)–O(11)	1.24[a]	1.21	1.23	C(15)–C(16)–C(17)		113.1	113.1
O(10)–H(21)		0.97	1.00	C(5)–C(9)–O(10)	118[a]	113.1	114.5
$CH_{(ring)average}$		1.08	1.08	C(5)–C(9)–O(11)	122[a]	125.3	122.4
Intermolecular H bond lengths and angles				O(10)–C(9)–O(11)		121.7	123.1
O–H···O			1.66	C(9)–O(10)–H(21)		106.5	110.2
O···O			2.66	$CCH_{(ring)average}$		119.6	119.6
O–H···O			179.8				

[a] Taken from Refs. [24,25].

for monomer and dimer are determined at B3LYP/6-311++G(d,p) level. The optimized parameters are presented in Table 2 in accordance with the atom numbering scheme of the molecule shown in Fig. 1. The dimeric conformation of 4-BBA molecule is shown in Fig. S1 (Supplementary Information). The molecules are linked by short intermolecular and asymmetric O–H···O hydrogen bonds of 1.66 Å between oxygen atom and hydroxyl group of another molecule to give rise to a dimer. Then, in order to test the effect of intermolecular interactions, the 4-BBA dimer formed by O–H···O intermolecular hydrogen bonds is investigated by theoretical methods. The computed value of O–H, O–H···O, O···O bond distances and O–H···O bond angle are 1.00, 1.66, 2.66 Å and 179.8°, respectively. The geometry of the molecule under investigation is considered by possessing C_1 point group symmetry. To the best of our knowledge, exact experimental data of the geometrical parameters of 4-BBA are not available in the literature. Therefore, our optimized structural parameters are compared with the XRD data of closely related molecules benzoic acid and butyric acid [24,25]. From the structural data, it is observed that the various C–C bond distances calculated between the ring carbon atoms and butyl group carbon atoms of monomer and dimer are found to be nearly the same with that of the experimental parameters. With the electron donating substituents on the benzene ring, the symmetry of the ring is distorted, yielding ring angles smaller than 120° at the point of substitution and slightly larger than 120° at the other positions [26]. It is evident from the calculated bond angles of C1–C2–C3 = 118° and C4–C5–C6 = 119.2° for both monomer and dimer models, shown in Table 2. The butyl group is slightly distorted with the benzene ring, because there is no conspicuous difference of the C–C bond length of the benzene ring, but slightly higher bond length of C2–C14, C14–C15, C15–C16 and C16–C17 bonds as compared to the C–C bonds on the benzene ring. It could be attributed to the steric effect of the larger butyl group. The C5–C9 bond length of 4-BBA is also longer, where the –COOH group is attached. This is due to the electron withdrawing nature of carboxylic acid group. The small difference between experimental and theoretical bond lengths and bond angles may be due to the presence of intermolecular hydrogen bonding.

5.2. Vibrational analysis

Vibrational spectroscopy is one of the most useful experimental tools for study of hydrogen bonded complexes. So the information on calculated harmonic vibrational frequencies can be useful. In our present study, we have performed a frequency calculation analysis to obtain the spectroscopic signature of 4-butyl benzoic acid for monomer and dimer. The 4-BBA molecule consists of 27 atoms therefore they have 75 vibrational normal modes. All the

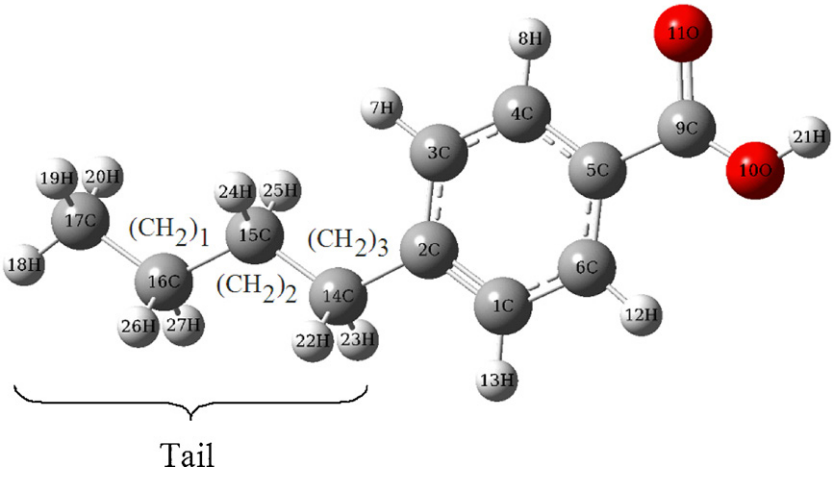

Fig. 1. The theoretical optimized geometric structure with atoms numbering of 4-BBA.

Table 3
Comparison of the experimental and calculated vibrational wavenumbers and proposal assignments of 4-BBA.

Mode nos.	Experimental wavenumbers (cm^{-1})		Theoretical wavenumbers (cm^{-1}) B3LYP/6-311++G(d,p)					Assignments
	FT-IR	FT-Raman	Unscaled	Scaled	I_{IR}	SA_{Raman}	I_{Raman}	TED (≥10%)
1			3773	3615	105.81	159.02	0.04	ν OH (100)
2		3072	3207	3072	1.57	99.38	0.05	$\nu\ (CH)_{ring}$ (96)
3			3198	3064	2.23	85.24	0.05	$\nu\ (CH)_{ring}$ (99)
4		3035	3163	3030	9.89	77.37	0.04	$\nu\ (CH)_{ring}$ (99)
5		3012	3161	3029	12.84	68.08	0.09	$\nu\ (CH)_{ring}$ (97)
6	2954	2960	3085	2956	44.57	138.51	0.02	ν_{asym} CH of CH_3 (99)
7			3081	2951	69.36	25.41	0.02	ν_{asym} CH_2 of CH_3 (85) + $\nu_{asym}\ (CH_2)_1$ (10)
8	2935	2931	3065	2937	27.03	33.48	0.00	$\nu_{asym}\ (CH_2)_3$ (64) + $\nu_{asym}\ (CH_2)_2$ (26)
9	2920		3042	2914	4.56	4.09	0.05	$\nu_{asym}\ (CH_2)_{1,2,3}$ (95)
10	2898	2896	3024	2897	56.62	63.58	0.09	$\nu_{sym}\ (CH_2)_3$ (57) + ν CH of $(CH_2)_{1,2}$ (37)
11			3023	2896	17.79	120.77	0.19	ν_{asym} CH of $(CH_2)_{1,2}$ (77) + $\nu_{sym}\ (CH_2)_3$ (19)
12			3020	2893	31.01	266.89	0.01	ν_{sym} CH_3 (92)
13	2870	2872	3010	2883	12.21	11.36	0.13	$\nu_{sym}\ (CH_2)_{1,2,3}$ (96)
14	2858	2851	3003	2877	7.64	172.06	0.23	$\nu_{sym}\ (CH_2)_{1,2}$ (99)
	2725							Overtone + combination
	2670							Overtone + combination
	2599							Overtone + combination
	2553							Overtone + combination
15	1690		1782	1707	442.41	155.24	1.00	ν C=O (82)
16	1610	1613	1649	1621	80.17	227.86	0.02	$\nu\ (CC)_{ring}$ (82)
17	1576	1581	1607	1579	6.97	3.56	0.01	$\nu\ (CC)_{ring}$ (75)
18	1514		1540	1514	2.58	1.04	0.00	β $(CH)_{ring}$ (55) + $\nu\ (CC)_{ring}$ (29)
19			1512	1487	8.22	0.43	0.05	ρ $\{(CH_2)_{1,2,3} + CH_3\}$ (64)
20		1475	1502	1476	1.98	7.52	0.06	ρ $\{(CH_2)_{1,2,3} + CH_3\}$ (65)
21			1499	1474	8.26	8.47	0.01	t CH_2 of CH_3 (88)
22	1466	1456	1490	1465	0.15	2.17	0.24	ρ $\{(CH_2)_{1,3} + CH_3\}$ (51)
23	1457	1442	1486	1460	0.89	34.85	0.02	ρ $(CH_2)_{1,2,3}$ (75)
24	1428	1419	1444	1419	18.29	2.25	0.00	β $(CH)_{ring}$ (35) + $\nu\ (CC)_{ring}$ (32)
25			1414	1390	3.11	0.33	0.05	w CH_3 (96)
26	1374	1363	1388	1365	0.39	6.24	0.18	w $(CH_2)_{1,2}$ (65)
27			1363	1340	133.38	21.29	0.26	β O–H (30) + ν C–O (24) + ν C–COOH (16)
28			1355	1332	2.07	30.61	0.05	w $(CH_2)_{1,3}$ (51)
29		1330	1352	1329	10.69	5.37	0.01	$\nu\ (CC)_{ring}$ (59) + t $(CH_2)_3$ (13)
30	1321	1317	1338	1315	3.29	1.12	0.10	β $(CH)_{ring}$ (59) + $\nu\ (CC)_{ring}$ (21)
31	1295		1330	1307	1.46	11.58	0.01	t $(CH_2)_{1,2}$ (65)
32		1286	1303	1281	0.01	1.05	0.05	t $(CH_2)_{1,2,3}$ (63)
33	1245	1255	1280	1258	0.24	5.10	0.02	w $(CH_2)_{1,2,3}$ (58)
34		1209	1230	1209	0.56	1.85	0.25	r $\{(CH_2)_{1,2} + CH_3\}$ (60) + t $(CH_2)_3$ (12)
35	1206		1225	1204	1.62	22.45	0.21	ν C–$(CH_2)_3$ (35) + $\nu\ (CC)_{ring}$ (30)
36		1181	1216	1195	65.83	18.46	0.81	β $(CH)_{ring}$ (38) + $\nu\ (CC)_{ring}$ (26) + β O–H (21)
37	1179		1189	1168	208.63	68.95	0.02	β $(CH)_{ring}$ (37) + β O–H (24) + $\nu\ (CC)_{ring}$ (11) + ν C–COOH (10)
38	1128	1132	1143	1123	1.84	1.97	0.45	β $(CH)_{ring}$ (51) + $\nu\ (CC)_{ring}$ (23)
39	1104	1105	1118	1099	18.55	33.03	0.04	r CH_3 (27) + β $(CCC)_{tail}$ (25) + $\nu\ (CC)_{tail}$ (23)
40			1104	1085	115.72	2.66	0.01	ν C–O (34) + $\nu\ (CC)_{ring}$ (16)
41	1070		1086	1067	71.00	0.82	0.18	$\nu\ (CC)_{ring}$ (21) + ν C–O (14) + t $\{C–(CH_2)_3\}$ (12)
42			1052	1034	0.88	11.61	0.00	$\nu\ (CC)_{tail}$ (89)
43	1020		1036	1018	16.58	0.23	0.08	ring deformation (94)
44			1005	988	2.79	4.81	0.00	$\nu\ (CC)_{tail}$ (81)
45	984		998	981	0.23	0.14	0.01	γ $(CH)_{ring}$ (79)
46	947		985	968	0.36	0.35	0.00	γ $(CH)_{ring}$ (68)
47			935	919	0.11	0.09	0.28	r $\{(CH_2)_3 + CH_3\}$ (43) + t $(CH_2)_{1,2}$ (29)
48	905	904	915	899	2.79	12.64	0.16	$\nu\ (CC)_{tail}$ (30) + r CH_3 (26)
49	855	861	866	851	10.14	6.57	0.01	γ $(CH)_{ring}$ (61)
50	834	837	855	841	0.49	0.47	0.66	γ $(CH)_{ring}$ (95)
51		817	837	823	0.55	23.76	0.01	$\nu\ (CC)_{ring}$ (36) + ν $\{(CH_2)_3–C_{ring}\}$ (16)
52	783	781	796	782	0.61	0.29	0.25	r $\{(CH_2)_{1,2,3} + CH_3\}$ (59)
53	762		785	772	38.56	7.53	0.18	γ CCOH (39) + γ $(CCC)_{ring}$ (24)
54	732		741	729	39.37	5.09	0.00	ν C–O (18) + ν $(C_{ring}–COOH)$ (12)
55			735	723	1.97	0.01	0.04	r $\{(CH_2)_{1,2,3} + CH_3\}$ (77)
56	702	705	719	707	37.10	0.89	0.29	γ $(CCC)_{ring}$ (46) + γ CCOH (21)
57	636	639	651	640	0.61	6.68	0.04	ring deformation (71)
58			622	611	30.09	0.77	0.09	β O–C=O (40) + β $(CCC)_{ring}$ (12)
59	549		577	568	43.48	1.52	0.12	γ OH (74)
60	520		522	513	48.74	1.68	0.06	γ $(CCC)_{ring}$ (28) + γ OH (13) + β $(CCC)_{tail}$ (10)
61			505	496	8.30	0.65	0.00	r COOH (70)
62	414		417	410	0.31	0.01	0.08	γ $(CCC)_{ring}$ (97)
63		408	407	400	5.33	0.54	0.15	β $(CCC)_{tail}$ (25) + ν C–COOH (15) + ν $(CC)_{tail}$ (14) + β O–C=O (11)
64			389	382	4.87	0.99	0.03	β $(CCC)_{tail}$ (27) + γ $(CCC)_{ring}$ (15)
65		302	348	342	0.39	0.18	0.79	r $(CH_2)_3$ (61) + r COOH (12)
66		254	277	272	0.25	3.73	0.00	γ $(CCC)_{ring}$ (28) + ν $(CC)_{tail}$ (12)
67		237	241	237	0.05	0.02	0.01	τ CH_3 (91)
68		219	230	226	0.04	1.19	0.00	β $(CCC)_{tail}$ (35)
69		176	191	188	1.25	0.12	0.00	r COOH (80)

Table 3 (*Continued*)

Mode nos.	Experimental wavenumbers (cm^{-1})		Theoretical wavenumbers (cm^{-1}) B3LYP/6-311++G(d,p)					Assignments
	FT-IR	FT-Raman	Unscaled	Scaled	I_{IR}	SA_{Raman}	I_{Raman}	TED (≥10%)
70			130	128	0.09	0.56	0.00	$\gamma\,(CCC)_{ring}$ (40) + $\beta\,(CCC)_{tail}$ (29)
71		110	110	108	0.04	0.02	0.00	$\gamma\,(CCC)_{tail}$ (84)
72		86	70	69	0.13	0.14	0.01	$\gamma\,(CCC)_{tail}$ (71)
73			68	67	0.72	0.40	0.04	γ CCO (91)
74			42	42	0.00	1.82	0.12	$\gamma\,(CCC)_{ring}$ (48) + $\beta\,(CCC)_{tail}$ (19)
75			19	18	0.38	3.66	0.00	$\gamma\,(CH_2)_3$ (86)

I_{IR}, IR intensity (K $mmol^{-1}$), SA_{Raman}, Raman activity ($Å^4$ amu^{-1}), ν, stretching; β, in-plane-bending; γ, out-of-plane bending; r, rocking; w, wagging; ρ, scissoring; τ, torsion; t, twisting. The CH_2 groups are numbered according to Fig. 1.

frequencies are assigned in terms of fundamental, overtone and combination bands. The recorded (FTIR and FT-Raman) and calculated vibrational wavenumbers along with their relative intensities and probable assignments with TED of title molecule are given in Table 3. The theoretical spectra were obtained from the B3LYP/6-311++G(d,p) method using Lorentzian band shape with band width on half-height 10 cm^{-1}. This reveals good correspondence between theory and experiment in main spectral features. The experimental and theoretical spectra are shown in Fig. 2. In order to simulate H bonding through COOH group we also calculated the vibrational wavenumbers of dimeric form of title molecule. The computed wavenumbers for the dimer structure are also presented in Table S2 (Supplementary Information). The computed vibrational wavenumbers and the atomic displacements corresponding to the different normal modes are used for identifying the vibrational modes unambiguously. The calculated wavenumbers are usually higher than the corresponding experimental quantities, due to the combination of electron correlation effects and basis set deficiencies. After applying, the different scaling factors, the theoretical wavenumbers are in good agreement with experimental wavenumbers. In our present investigation, wavenumbers in the ranges from 4000 to 1700 cm^{-1} and lower than 1700 cm^{-1} are scaled with 0.958 and 0.983 respectively, [27].

5.2.1. C–H vibrations

The existence of one or more aromatic rings in a structure is normally readily determined from the C–H and C=C–C ring related vibrations. The substituted benzene like molecule gives rise to C–H stretching, C–H in-plane and C–H out-of-plane bending vibrations. The hetero aromatic structure shows the presence of C–H stretching vibration in the region 3100–3000 cm^{-1}, which is the characteristic region for the ready identification of C–H stretching vibration [28,29]. In this region, the bands are not affected appreciably by the nature of the substituent. The aromatic C – H stretching frequencies arise from the modes observed at 3062 (a_{1g}), 3047 (e_{2g}), 3060 (b_{1u}) and 3080 (e_{1u}) cm^{-1} of benzene and its derivatives [30]. In our present work, the C–H stretching vibrations are observed at 3072, 3035 and 3012 cm^{-1} in FT-Raman spectrum and there is no peaks observed in FTIR spectrum for C–H vibrations. The calculated values of these modes for the title molecule have been found to be 3072, 3064, 3030 and 3029 cm^{-1} for monomer and 3071, 3069, 3053, 3025 cm^{-1} for dimer at the DFT-B3LYP calculation level. As

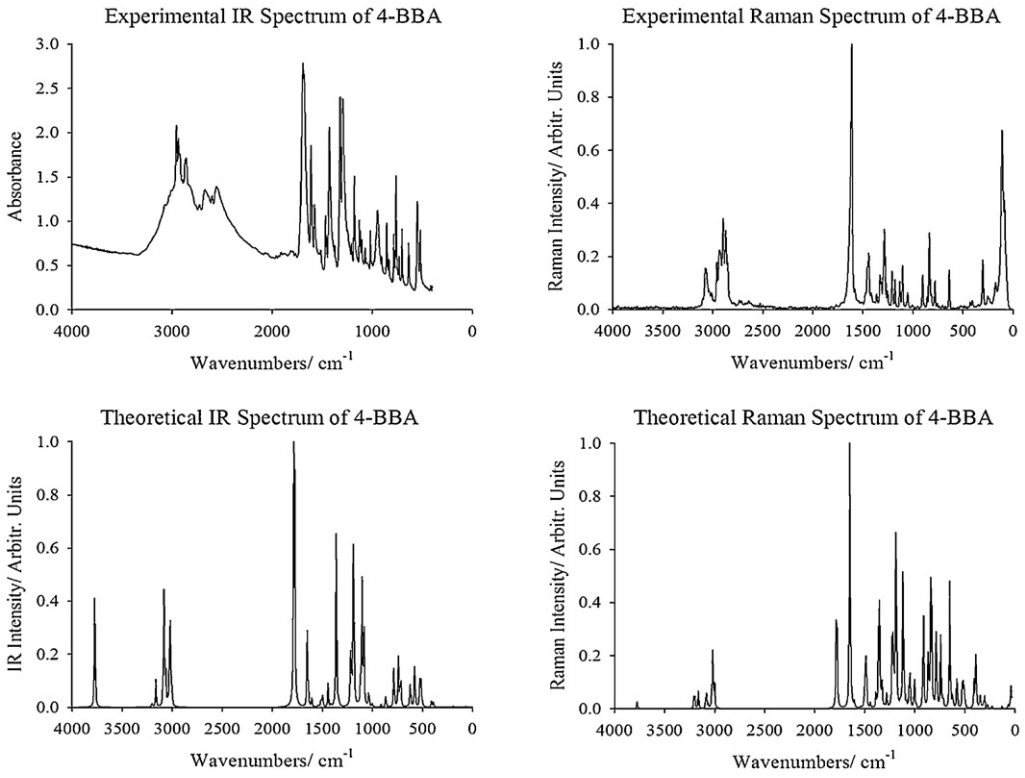

Fig. 2. Experimental and theoretical Infrared and Raman spectra of 4-BBA.

indicated by the TED, these four modes involve approximately 99% contribution suggesting that they are pure stretching modes. The asymmetric C–H stretching vibration of methyl group is observed at 2954 cm^{-1} in FTIR and at 2960 cm^{-1} in FT-Raman and the same vibration is predicted for monomer at 2956 cm^{-1} by B3LYP method. All the computed wavenumbers of both models are in line with the experimental wavenumbers.

The aromatic C–H in-plane bending modes of benzene and its derivatives are observed in the region 1300–1000 cm^{-1}, the bands are sharp but have weak-to-medium intensity. The C–H in-plane bending vibrations predicted at 1315, 1195, 1168 and 1123 cm^{-1} by B3LYP/6-311++G(d,p) method show excellent agreement with FTIR bands at 1321, 1179 and 1128 cm^{-1} and FT-Raman bands at 1317, 1181 and 1132 cm^{-1}. The C–H in-plane bending vibrations of dimer are predicted at 1307, 1190, 1185, 1184, 1121 cm^{-1}. The aromatic C–H in-plane bending vibrations have substantial overlapping with the ring C–C stretching vibrations. The absorption bands arising from C–H out-of-plane bending vibrations are usually observed in the region at 1000–675 cm^{-1} [31–35]. The C–H out-of-plane bending vibrations are observed as medium bands in FTIR at 984, 947, 855, 834 cm^{-1} and Raman active mode can be observed as medium bands in Raman spectrum at 861, 837 cm^{-1}. This also shows good agreement with theoretically scaled harmonic wavenumber values of both monomer at 981, 968, 851 and 841 cm^{-1} and dimer at 983, 974, 852, 851, 843 cm^{-1} by B3LYP/6-311++G(d,p) method.

5.2.2. Methylene group vibrations

The C–H stretching of the methylene groups are at lower frequencies than those of the aromatic C–H ring stretching. The CH_2 antisymmetric stretching vibrations are generally observed in the region 3000–2900 cm^{-1}, while the CH_2 symmetric stretch will appear between 2900 and 2800 cm^{-1} [36,37]. The CH_2 antisymmetric and symmetric stretching vibrations were observed at 2935, 2920 and 2898, 2870, 2858 cm^{-1} (FTIR) and 2931 cm^{-1} and 2896, 2872, 2851 cm^{-1} (FT-Raman), respectively for 4-BBA molecule. The calculated antisymmetric and symmetric CH_2 stretching vibrations of the methylene group are at 2937, 2914 and 2897, 2896, 2883, 2877 cm^{-1} (monomer), respectively (mode nos. 8–11, 13 and 14) by B3LYP method. For dimer molecule, the antisymmetric and symmetric CH_2 stretching vibrations are found to be 2956, 2952, 2925 cm^{-1} and 2887, 2877, 2875 cm^{-1} by the same method. Compared with the experimental data, the predicted values of monomer are better reproduced than the dimer. In the present assignment, the CH_2 bending modes follow, in decreasing frequency, the general order CH_2 deformation > CH_2 scis > CH_2 wagg > CH_2 twist > CH_2 rock. Since the bending modes involving the hydrogen atom attached to the central carbon atom falls in the 1450–875 cm^{-1} range, there is extensive vibrational coupling of these modes with CH_2 deformations, particularly with the CH_2 twist. It is of some note that both ρCH_2 and rCH_2 were sensitive to the molecular conformation. The recorded spectrum shows only two medium strong peaks at 1466, 1457 cm^{-1} (FTIR) and at 1456, 1442 cm^{-1} (FT-Raman) are assigned to CH_2 scissoring vibrations. The computed values of both models show good agreement with the above experimental data. From the theoretical calculations, the CH_2 wagging modes are predicted at 1365, 1332, 1258 cm^{-1} (monomer) (mode nos. 26, 28, and 33). It shows excellent correlation with the FTIR and FT-Raman bands at 1374, 1245 and 1363, 1255 cm^{-1}, respectively and also shows the maximum TED contribution of 96%. The peaks observed at 1295 cm^{-1} in FTIR and at 1286 cm^{-1} in FT-Raman and the calculated wavenumbers 1307, 1281 cm^{-1} (monomer) and 1315, 1298 cm^{-1} (dimer) are assigned to CH_2 twisting vibrations. The CH_2 rocking vibrations are also predicted at lower wavenumbers with good correlation of experimental data.

5.2.3. Methyl group vibrations

The title molecule 4-BBA under consideration possesses one CH_3 unit which lies in the terminal group of molecule. For the assignments of CH_3 group frequencies, nine fundamentals can be associated to each CH_3 group [38]. The C–H stretching in CH_3 occurs at lower frequencies than those of aromatic ring (3100–3000 cm^{-1}). Moreover, the asymmetric stretch is usually at higher wavenumber than the symmetric stretch. Methyl group vibrations are generally referred to as electron-donating substituent in the aromatic rings system, the antisymmetric C–H stretching mode of CH_3 is expected around 2980 cm^{-1} and CH_3 symmetric stretching is expected at 2870 cm^{-1} [39,40]. The first of these results from the antisymmetric stretching of CH_3 mode in which the two C–H bonds of the methyl group are expanding while the third one is contracting. The second arises from the symmetric stretching, in which all the three C–H bonds expand and contract in phase. The CH_3 symmetric stretching mode is predicted by B3LYP method at 2893 cm^{-1} for both the case, it shows above 90% of TED contribution suggesting that it is a pure stretching mode. There is no peak observed for CH_3 stretching vibration in both FTIR and FT-Raman spectra.

For methyl substituted benzene derivatives, the antisymmetric and symmetric deformation vibrations of methyl group normally appear in the region 1465–1440 cm^{-1} and 1390–1370 cm^{-1}, respectively [41–43]. The band at 1466 cm^{-1} in FTIR and the bands at 1475, 1456 cm^{-1} in FT-Raman are attributed to CH_3 scissoring vibrations. The calculated vibrations are coupled with the CH_2 scissoring vibrations with appreciable contribution of TED. The wagging vibrations of the CH_3 group in 4-BBA appear as independent vibrations. The wavenumber at 1390 cm^{-1} in monomer and at 1392 cm^{-1} in dimer is assigned to CH_2 wagging vibration. The torsional mode of CH_3 vibration is measured at 237 cm^{-1} in FT-Raman spectrum and it exactly correlates with the theoretically predicted monomeric value of 237 cm^{-1} and dimeric value of 242, 241 cm^{-1}.

5.2.4. Carboxylic acid (–COOH) group vibrations

The vibrational bands of the terminal –COOH groups of 4-BBA contain the C–O, C=O and O–H vibrational modes. C=O stretching band appears strongly in the region 1870–1540 cm^{-1} in which the position of C=O stretching band depends on the physical state, electronic and mass effects of neighboring substituents, conjugations and intramolecular and intermolecular hydrogen bonding [31,44–46]. The C=O stretching mode is the strongest band in the infrared spectrum and appears with diminished intensity in the Raman spectrum. Hence the very strong FTIR band observed at 1690 cm^{-1} is assigned to the C=O stretching band of 4-BBA molecule. The similar vibration is calculated for dimer at 1654 cm^{-1} by DFT-B3LYP method. However, the computed value (1707 cm^{-1}) of C=O stretching vibration of monomer shows better agreement with the experimental data than dimer.

As for the –OH hydroxyl group which connects the molecules, the observed IR frequency region is usually at the interval 3550–3200 cm^{-1} [46]. Although these values are not observed in the recorded IR and Raman spectra shown in Fig. 2, the O–H stretching mode of monomer is found as 3615 cm^{-1} by B3LYP calculation level, as given in Table 3. Diverse dimeric units are common features among mono aminobenzoic acids as well as they are observed in the structure of benzoic acid [47]. It can be observed that there is a frequency downshift of O–H stretching vibration in dimer due to the presence of intermolecular interaction. The occurrence of dimeric conventions is due to hydrogen bonds which act as the bridging mode. The lower stretching frequency observed in 4-BBA compared with the free O–H group stretching signifies that there is a possibility of intermolecular hydrogen bonding in 4-BBA, between the hydroxyl group of one molecule and carbonyl group of another molecule. The carboxylic acids show in-plane and out-of-plane bending band of O–H near 1179 and 549 cm^{-1} (FTIR). The TED

Table 4
The observed (in DMSO) and predicted ^{1}H and ^{13}C NMR isotropic chemical shifts (with respect to TMS, all values in ppm) for 4-BBA.

Atom	Experimental	B3LYP/6-311++G(d,p)		Atom	Experimental	B3LYP/6-311++G(d,p)	
	DMSO	Gas phase	DMSO		DMSO	Gas phase	DMSO
H(7)	7.31	7.41	7.58	C(1)	128.90	132.58	133.72
H(8)	7.85	8.35	8.29	C(2)	148.19	154.47	157.45
H(12)	7.85	8.16	8.23	C(3)	128.90	128.12	128.87
H(13)	7.31	7.35	7.58	C(4)	129.80	137.83	136.83
H(18)	0.89	1.25	1.22	C(5)	128.74	129.87	128.76
H(19)	0.89	1.01	1.00	C(6)	129.80	135.88	135.74
H(20)	0.89	1.01	1.00	C(9)	167.76	170.43	172.60
H(21)	3.37	5.50	6.12	C(14)	35.21	37.85	37.79
H(22)	2.64	2.84	2.94	C(15)	33.19	31.70	31.41
H(23)	2.64	2.84	2.94	C(16)	22.16	27.92	27.49
H(24)	1.56	1.60	1.63	C(17)	14.17	15.53	15.13
H(25)	1.56	1.60	1.63				
H(26)	1.30	1.35	1.39				
H(27)	1.30	1.35	1.39				

calculations show that the hydroxyl stretching vibrational mode is very pure. But the in-plane bending vibration of the hydroxyl group is overlapped with the other vibrations. The band due to the free hydroxyl group is sharp and its intensity increases. In addition carboxylic acids also show C–O stretching band in FTIR at about 1070 cm^{-1}.

5.2.5. Ring vibrations

The aromatic ring vibrational modes of title compound have been analyzed based on the vibrational spectra of previously published vibrations of the benzene molecule are helpful in the identification of the phenyl ring modes [32,34]. The ring stretching vibrations are very prominent, as the double bond is in conjugation with the ring, in the vibrational spectra of benzene and its derivatives [31]. The carbon–carbon stretching modes of the phenyl group are expected in the range from 1650 to 1200 cm^{-1}. The actual position of these modes is determined not so much by the nature of the substituents but by the form of substitution around the ring [30]. In general, the bands are of variable intensity and are observed at 1625–1590, 1590–1575, 1540–1470, 1465–1430 and 1380–1280 cm^{-1} from the wavenumber ranges given by Varsanyi [48] for the five bands in the region. In the present work, the wavenumbers observed in the FTIR spectrum at 1610, 1576, 1514, 1428, 1321 cm^{-1} and in FT-Raman spectrum at 1613, 1581, 1419, 1330, 1317 cm^{-1} have been assigned to C–C stretching vibrations. The theoretically computed values at 1621, 1579, 1514, 1419, 1329, 1315 cm^{-1} (monomer) show an excellent agreement with experimental data. These modes are mixed mode with the contribution of C–H in-plane bending vibration in this region. The calculated values (1622–1307 cm^{-1}) of dimer molecule are also in good agreement with the experimental values. The C–C–C out-of-plane bending modes of monomer is attributed to the low wavenumbers computed at 707, 513, 410 cm^{-1} and these wavenumbers are consistent with the experimental wavenumbers.

In butyl group, the C–C stretching vibrations are observed at 1104, 905 cm^{-1} in FTIR spectrum and at 1105, 904 cm^{-1} in FT-Raman spectrum. The same vibrations are predicted for monomer at 1099, 1034, 988, 899 cm^{-1} and for dimer at 1095, 1046, 1006, 894 cm^{-1} by B3LYP/6-311++G(d,p) method. The C–C–C in-plane and out-of-plane bending vibrations are also computed theoretically and the correlation between the experimental and theoretical values are observed.

5.3. NMR spectral analysis

The ^{13}C and ^{1}H theoretical and experimental chemical shifts, isotropic shielding tensors and the assignments of 4-BBA are presented in Table 4. The experimental ^{13}C, ^{1}H and DEPT NMR spectra are shown in Figs. 3–5. ^{1}H atom is mostly localized on periphery of the molecules and their chemical shifts would be more susceptible to intermolecular interactions in the aqueous solutions as compared to that for other heavier atoms. Aromatic carbons give signals in overlapped areas of the spectrum with chemical shift values from 100 to 150 ppm [49,50]. In our present investigation, the experimental chemical shift values of aromatic carbons except C2 are in the range 128.74–129.80 ppm. The chemical shift of C2 (148.19 ppm) is greater than the other aromatic carbons because of the substitution of butyl group. The positions of carboxylic groups are recognized, whereas the localization of proton is not. The ^{13}C chemical shifts of carboxylic acids are in the range of 160–182 ppm but those of their salts between 167 and 183 ppm [51]. The experimental chemical shift value of C9 is 167.76 ppm and the calculated value is 170.43 ppm in gas phase and 172.60 ppm in DMSO solvent. The C9 and H21 atoms are deshielded due to the presence of electronegative oxygen in the carboxylic group. Besides, due to shielding effect which the non-electronegative property of hydrogen atom, the chemical shift value of C17 atom is lower than the others carbon peak. In the ^{13}C NMR spectrum, the C14, C15 and C16 (methylene carbons) signals are observed at 35.21, 33.19 and 22.16 ppm respectively. Similarly, the corresponding proton (in methylene groups) chemical shifts are in the range 2.64–1.30 ppm.

^{1}H chemical shifts of 4-BBA were obtained by complete analysis of their NMR spectra and interpreted critically in an attempt to quantify the possible different effects acting on the shielding constant of protons. The chemical shift values of aromatic protons are in the range 7.31–7.85 ppm. The H7 and H13 values are slightly smaller than the H8 and H12 values. Because, the electron donating butyl group cause shielding of the aromatic protons. The hydrogen atoms present in the ortho positions to butyl group experience little more shielding than other aromatic hydrogen atoms. Hydrogen attached or nearby electron donating atom or group increases the shielding and moves the resonance towards to a lower frequency. The chemical shifts obtained and calculated for the hydrogen atoms of methyl groups are quite low. All values are $\leq$3 ppm [52] due to shielding effect. It is correct from above literature data, in our present study the methyl protons at C17 appears at 0.89 ppm shows good agreement with computed chemical shift values. The chemical shift of proton (H21) attached to the electron withdrawing group is 3.37 ppm and the deviation between experimental and computed chemical shifts may be due to the presence of intermolecular hydrogen bonding. The correlation graphics between the experimental and calculated ^{13}C NMR and ^{1}H NMR chemical shifts of 4-BBA are presented in Fig. 6.

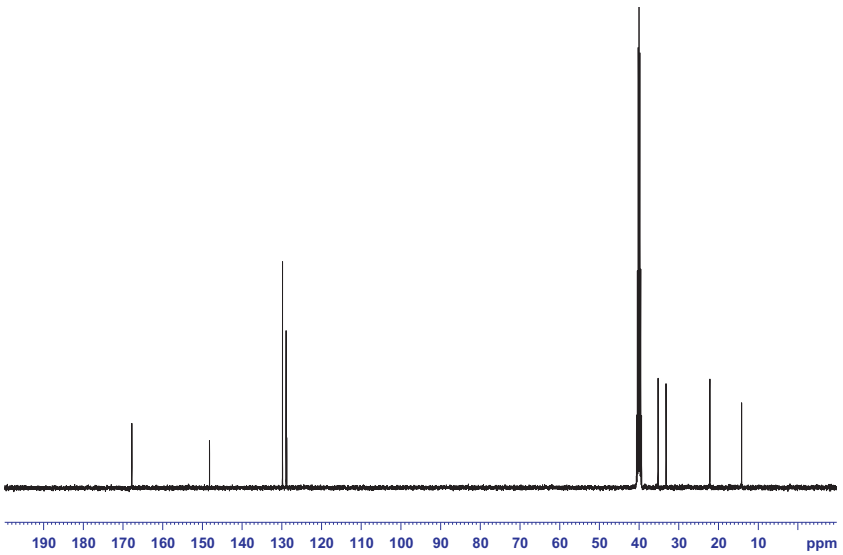

Fig. 3. Experimental ^{13}C NMR spectrum of 4-BBA.

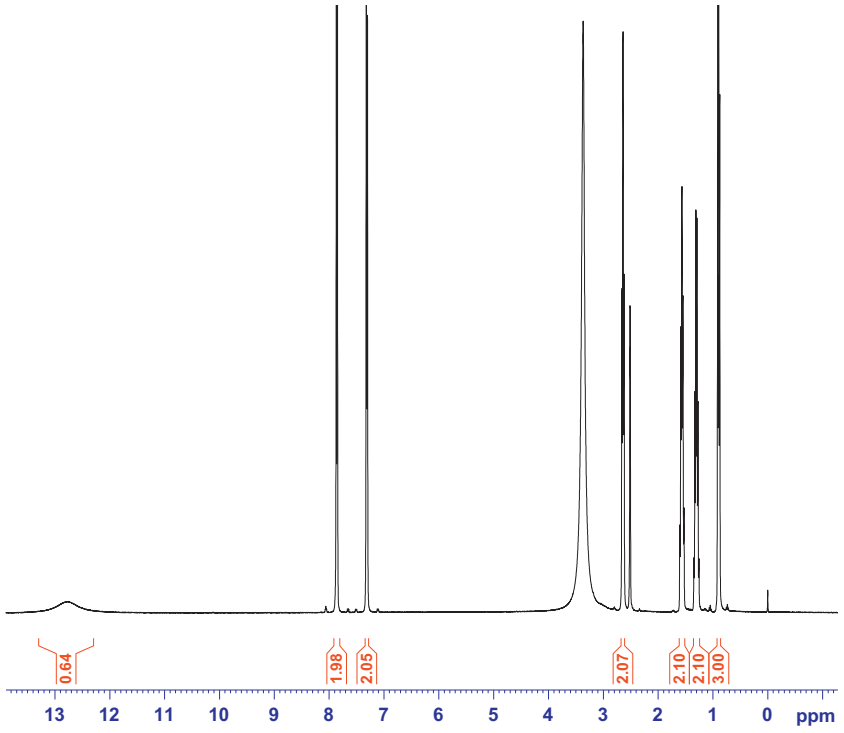

Fig. 4. Experimental ^{1}H NMR spectrum of 4-BBA.

5.4. Electronic properties

5.4.1. Absorption spectra

Molecules allow strong π–π^* and σ–σ^* transition in the UV–vis region with high extinction coefficients. Ultraviolet spectra analyses of 4-BBA have been researched by theoretical calculation. The electronic absorption spectra of title molecule were measured in ethanol and water at room temperature. The excitation energies, absorbance and oscillator strengths for the title molecule at the optimized geometry in the ground state were obtained in the framework of TD-DFT calculations with the B3LYP/6-311++G(d,p) method. It is obvious that to use TD-DFT calculations to predict the electronic absorption spectra is a quite reasonable method. The theoretical and experimental maximum absorption wavelengths are compared in Table 5. TD-DFT methods are computationally more expensive than semi-empirical methods but allow easily studies of medium size molecules [53,54]. Briquet and Vercauteren reported that TD-DFT λ_{max} calculations by 6-311++G(d,p) basis set is compatible with experimental results [55]. Test calculations have shown that the inclusion of extra polarization functions does not affect the excitation energies, besides the addition of diffuse functions leads to an increase in computation time. Experimentally determined maximum absorption values are 237 nm (in ethanol) and 238 nm (in water). λ_{max} values obtained with B3LYP/6-311++G(d,p) are 255, 252, 240 nm (in gas phase), 258, 246, 245 nm (in ethanol) and 258, 246, 245 nm (in water). The

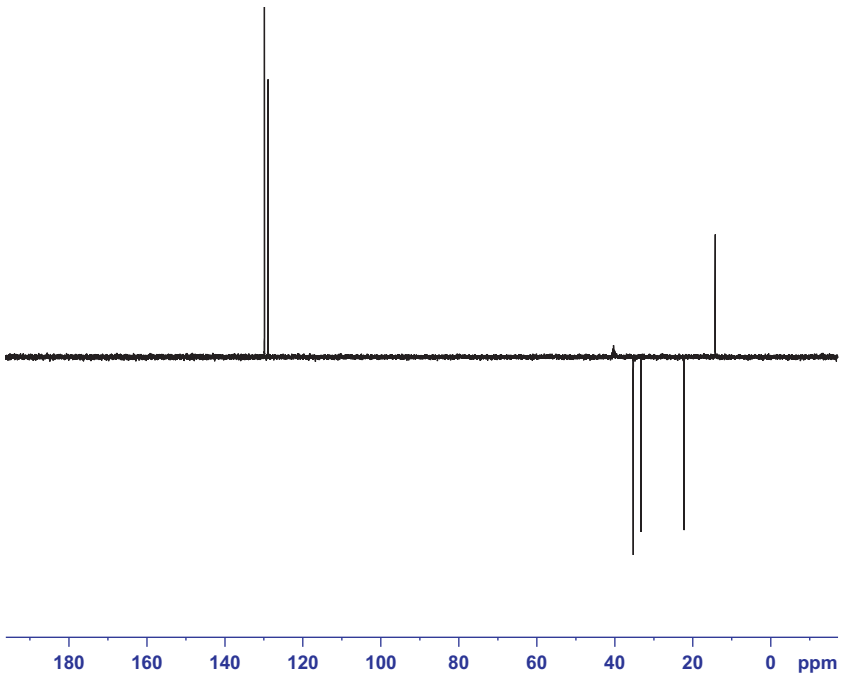

Fig. 5. Experimental DEPT NMR spectrum of 4-BBA.

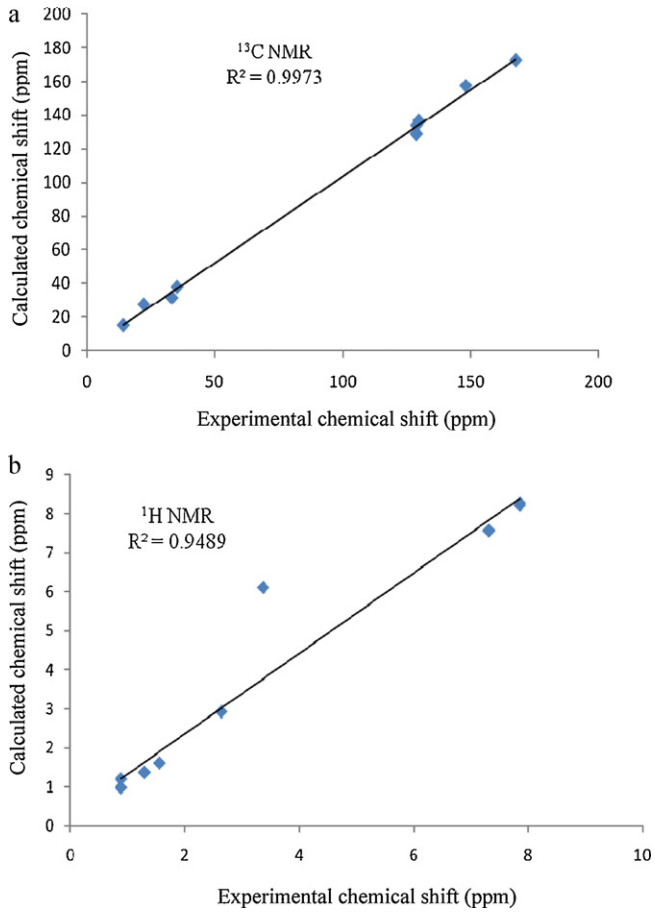

Fig. 6. . The linear regression between the experimental and theoretical ^{13}C and ^{1}H NMR chemical shifts of 4-BBA.

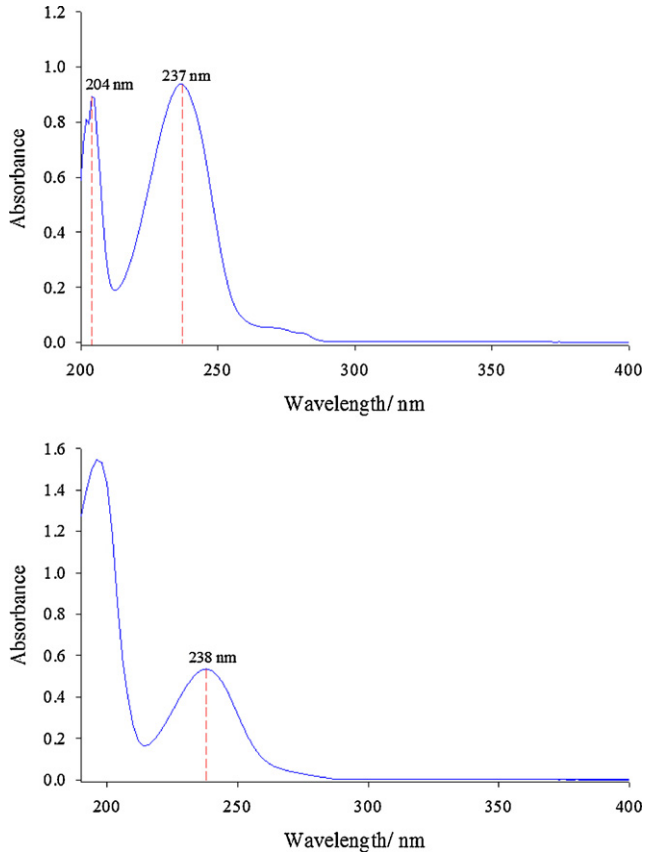

Fig. 7. Experimental UV–vis spectra of 4-BBA in ethanol (top) and water (bottom) solution.

experimental absorption spectra are shown in Fig. 7. While agreement between the calculated and experimental λ_{max} values of 4-BBA is evident, the calculated bands are blue-shifted by ~7 and ~2 nm.

Table 5
The experimental and computed absorption wavelength λ (nm), excitation energies *E* (eV), absorbance and oscillator strengths (*f*) of 4-BBA in gas phase, ethanol and water solution.

Experimental						TD-DFT/B3LYP/6-311++G(d,p)								
Ethanol			Water			Gas			Ethanol			Water		
λ (nm)	*E* (eV)	Abs.	λ (nm)	*E* (eV)	Abs.	λ (nm)	*E* (eV)	*f* (a.u.)	λ (nm)	*E* (eV)	*f* (a.u.)	λ (nm)	*E* (eV)	*f* (a.u.)
						255.10	4.8602	0.0148	258.16	4.8026	0.0260	258.21	4.8017	0.0256
						252.98	4.9009	0.0000	246.94	5.0209	0.4436	246.92	5.0212	0.4389
237	5.2161	0.536	238	5.2381	0.938	240.38	5.1578	0.3503	245.78	5.0444	0.0000	245.49	5.0504	0.0000

5.4.2. Frontier molecular orbital analysis

Many organic molecules that contain conjugated π-electrons are characterized as hyper-polarizabilities and are analyzed by means of vibrational spectroscopy [56,57]. According to the TD-DFT calculated electronic absorption spectra, the maximum absorption wavelength corresponding to the electronic transition is from the highest occupied molecular orbital (HOMO) to the lowest unoccupied molecular orbital (LUMO). The frontier molecular orbital energies and corresponding density of state of the title compound is shown in Fig. 8(a) and (b). The energies of four important molecular orbitals of 4-BBA: the highest, second highest and third highest occupied molecular orbitals (HOMO, HOMO-1 and HOMO-2), the lowest unoccupied molecular orbital (LUMO) were calculated and are presented in Table 6. The lowest singlet → singlet spin-allowed excited states of 4-BBA were taken into account for the TD-DFT calculation in order to investigate the properties of electronic absorption. The energy gap between HOMO and LUMO is a critical parameter in determining molecular electrical transport properties [58].

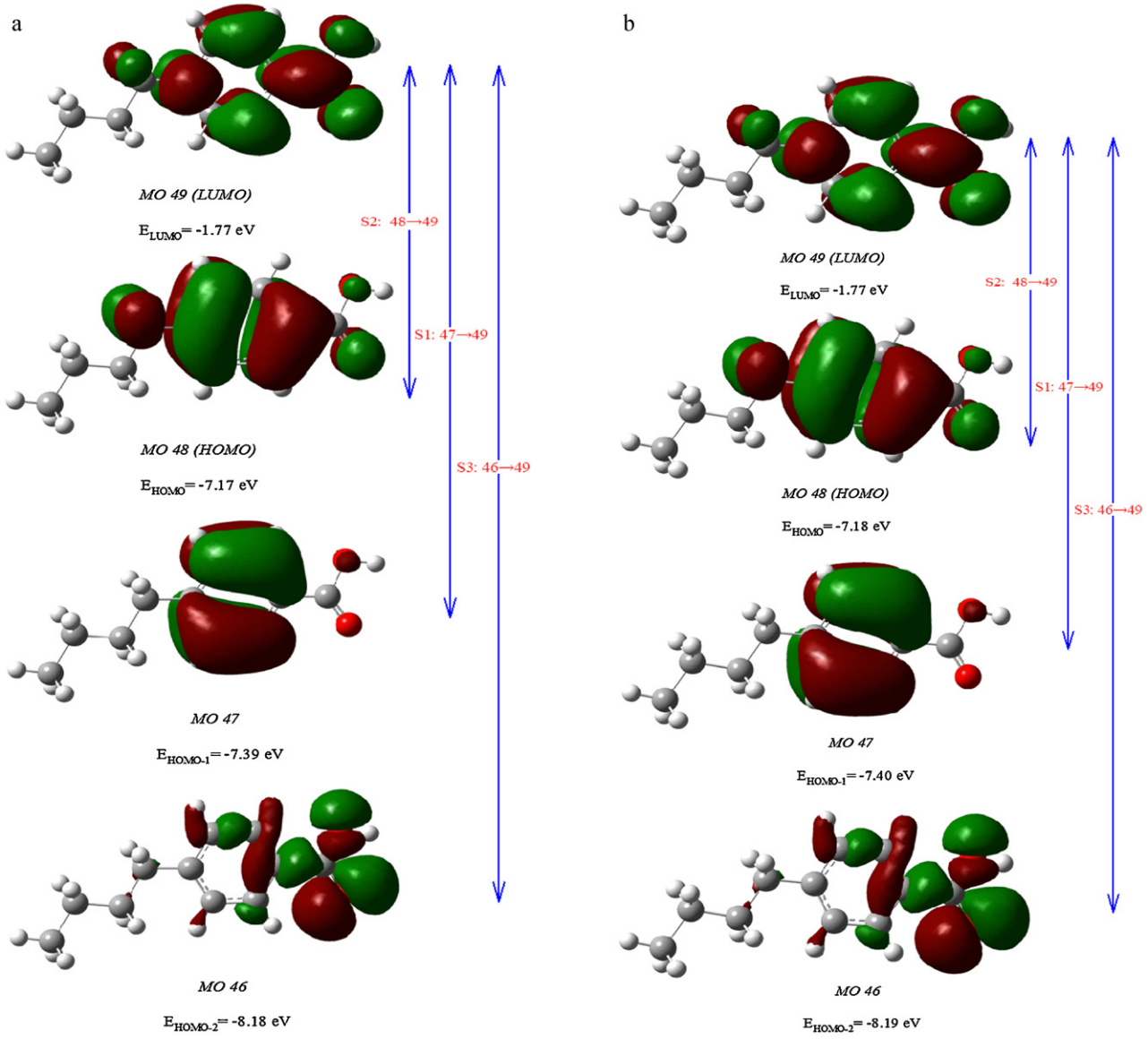

Fig. 8. (a) Patterns of the principle highest occupied and lowest unoccupied molecular orbitals of 4-BBA obtained with TD-DFT/6-311++G(d,p) method in ethanol. (b) Patterns of the principle highest occupied and lowest unoccupied molecular orbitals of 4-BBA obtained with TD-DFT/6-311++G(d,p) method in water.

Table 6
Calculated energy values of 4-BBA for ground state in gas phase, and ethanol and water solutions.

TD-DFT/B3LYP	Gas	Ethanol	Water
E_{total} (Hartree)	−578.2478	−578.2556	−578.0795
E_{HOMO} (eV)	−7.12	−7.17	−7.18
E_{LUMO} (eV)	−1.64	−1.77	−1.77
$\Delta E_{HOMO-LUMO\ gap}$ (eV)	−5.48	−5.41	−5.40
E_{HOMO-1} (eV)	−7.34	−7.39	−7.40
E_{HOMO-2} (eV)	−7.89	−8.18	−8.19
$\Delta E_{HOMO-1-LUMO\ gap}$ (eV)	−5.70	−5.63	−5.62
$\Delta E_{HOMO-2-LUMO\ gap}$ (eV)	−6.25	−6.41	−6.42

The lowest unoccupied molecular orbital (LUMO) energy is −1.64 eV (in gas phase), −1.77 eV (in ethanol) and −1.77 eV (in water) and the highest occupied molecular orbital (HOMO) energy is −7.12 eV (in gas phase), −7.17 eV (in ethanol) and −7.18 eV (in water). The energy gap of HOMO–LUMO explains the eventual charge transfer interaction within the molecule, and the frontier orbital energy gap of 4-BBA is found to be −5.48 eV (in gas phase), −5.41 eV (in ethanol) and −5.40 eV (in water) obtained at TD-DFT method using 6-311++G(d,p) basis set. The HOMO is localized on the benzene ring, –O–C=O part and methylene group [$(CH_2)_3$] attached to the ring and LUMO is contributed by the whole of the molecule without methyl group and methylene [$(CH_2)_1$ and $(CH_2)_2$] groups.

6. Conclusions

In the present work, we have calculated the geometric parameters, vibrational frequencies and ^{13}C and ^{1}H NMR chemical shifts of the 4-butyl benzoic acid molecule by using B3LYP method with 6-311++G(d,p) basis set. In order to take into account the effect of intermolecular interaction, the 4-BBA dimer formed by O–H···O intermolecular hydrogen bonds was investigated by theoretical methods. An excellent correlation between the experimental and the calculated wavenumbers in monomer model was obtained. Significant discrepancies have been found for a dimer model when the hydrogen bonds are involved. The calculations show that using TD-DFT/6-311++G(d,p) approach, experimental absorption spectrum has been well reproduced. It has been conclude that the lowest singlet excited state of the 4-BBA molecule is mainly derived from the HOMO → LUMO ($\pi \rightarrow \pi^*$) electron transition.

Appendix A. Supplementary data

Supplementary data associated with this article can be found, in the online version, at doi:10.1016/j.saa.2011.09.058.

References

[1] J.A. Pollard, Legislative aspects, in: N.J. Russel, G.W. Gould (Eds.), Food Preservatives, AVI Publishers, New York, 1991, p. 235.
[2] R. Swinslocka, M. Samsonowicz, E. Regulaska, W. Lewandowski, J. Mol. Struct. 792 (2006) 227–238.
[3] R.A. Sheldon, J.K. Kochi, Metal-Catalyzed Oxidations of Organic Compounds, Academic, New York, 1981.
[4] M. Hudlicky, Oxidation in Organic Chemistry ACS Monograph 186, American Chemical Society, Washington, DC, 1990.
[5] B.M. Trost, Comprehensive Organic Synthesis (Oxidation), Pergamon, New York, 1991.
[6] K. Kreutz, A. Schlossberg, U.S. Patent 6,395,720 B1 (2002).
[7] N. Sundaraganesan, B.D. Joshua, K. Settu, Spectrochim. Acta 66A (2007) 381–388.
[8] N. Sundaraganesan, S. Ilakiamani, B.D. Joshua, Spectrochim. Acta 67A (2007) 287–297.
[9] N. Sundaraganesan, B. Anand, C. Meganathan, B.D. Joshua, Spectrochim. Acta 69A (2008) 871–879.
[10] N. Sundaraganesan, B.D. Joshua, C. Meganathan, R. Meenashi, J.P. Cornard, Spectrochim. Acta 70A (2008) 376–383.
[11] M. Ramalingam, N. Sundaraganesan, H. Saleem, J. Swaminathan, Spectrochim. Acta 71A (2008) 23–30.
[12] C. Meganathan, S. Sebastian, M. Kurt, K.W. Lee, N. Sundaraganesan, J. Raman Spectrosc. 41 (2010) 1369–1378.
[13] D. Hatzipanayioti, K. Kontotheodorou, Spectrochim. Acta 78A (2011) 949–960.
[14] P.V. Kolinsky, Opt. Eng. 31 (1992) 1676–1684.
[15] D.F. Eaton, Science 253 (1991) 281–287.
[16] Gaussian Inc., Gaussian 03 Program, Gaussian Inc., Wallingford, 2004.
[17] R. Dennington I.I., T. Keith, J. Millam, Gauss View Version 4.1 2, Semichem, Inc., Shawnee Mission, KS, 2007.
[18] M.H. Jamróz, Vibrational energy distribution analysis, VEDA 4 computer program, Poland, 2004.
[19] R. Ditchfield, J. Chem. Phys. 56 (1972) 5688–5691.
[20] K. Wolinski, J.F. Hinton, P. Pulay, J. Am. Chem. Soc. 112 (1990) 8251–8260.
[21] G. Keresztury, S. Holly, J. Varga, G. Besenyei, A.Y. Wang, J.R. Durig, Spectrochim. Acta 9A (1993) 2007–2026.
[22] G. Keresztury, J.M. Chalmers, in: R. Griffith (Ed.), Raman Spectroscopy: Theory, Hand book of Vibrational Spectroscopy, vol. 1, John Wiley & Sons Ltd., New York, 2002.
[23] D.A. Kleinman, Phys. Rev. 126 (1962) 1977–1979.
[24] G.A. Sim, J.M. Robertson, T.H. Goodwin, Acta Cryst. 8 (1955) 157–164.
[25] F.J. Strieter, D.H. Templeton, Acta Cryst. 15 (1962) 1240–1244.
[26] Y. Wang, S. Saebar, C.U. Pittman, J. Mol. Struct. Theochem. 281 (1993) 91–98.
[27] N. Sundaraganesan, S. Illakiamani, H. Saleem, P.M. Wojciechowski, D. Michalska, Spectrochim. Acta 61A (2005) 2995–3001.
[28] V.K. Rastogi, M.A. Palafox, R.P. Tanwar, L. Mittal, Spectrochim. Acta A 58 (2002) 1987–2004.
[29] M. Silverstein, G.C. Basseler, C. Morill, Spectrometric Identification of Organic Compounds, Wiley, New York, 1981.
[30] L.J. Bellamy, The Infrared Spectra of Complex Molecules, 3rd ed., Wiley, New York, 1975.
[31] G. Varsanyi, Vibrational Spectra of Benzene Derivative, Academic Press, New York, 1969.
[32] N.B. Colthup, L.H. Daly, S.E. Wiberley, Introduction to Infrared and Raman Spectroscopy, Academic Press, New York, 1990.
[33] F.R. Dollish, W.G. Fateley, F.F. Bentley, Characteristic Raman Frequencies of Organic Compounds, John Wiley & Sons, New York, 1997.
[34] G. Socrates, Infrared Characteristic Group frequencies, Wiley-Interscience Publication, New York, 1980.
[35] B. Smith, Infrared Spectral Interpretation, A Systematic Approach, CRC Press, Washington, DC, 1999.
[36] D. Sajan, J. Binoy, B. Pradeep, K. Venkatakrishnan, V.B. Kartha, I.H. Joe, V.S. Jayakumar, Spectrochim. Acta 60A (2004) 173–180.
[37] S. Gunasekaran, S.R. Varadhan, K. Manoharan, Asian J. Phys. 2 (1993) 165–172.
[38] P.S. Kalsi, Spectroscopy of Organic Compounds, Wiley Eastern Limited, New Delhi, 1993.
[39] D. Sajan, I. Hubert Joe, V.S. Jayakumar, J. Raman Spectrosc. 37 (2005) 508–519.
[40] M. Gussoni, C. Castiglioni, M.N. Ramos, M.C. Rui, G. Zerbi, J. Mol. Struct. 224 (1990) 445–470.
[41] B.V. Reddy, G.R. Rao, Vib. Spectrosc. 6 (1994) 231–250.
[42] J.F. Areanas, I.L. Tocn, J.C. Otero, J.I. Marcos, J. Mol. Struct. 410 (1997) 443–446.
[43] D.A. Long, W.O. Jeorge, Spectrochim. Acta 19 (1963) 1777–1790.
[44] B.H. Stuart, Infrared Spectroscopy: Fundamentals and Applications, John Wiley & Sons, England, 2004.
[45] S. Chandra, H. Saleem, N. Sundaraganesan, S. Sebastian, Spectrochim. Acta A74 (2009) 704–713.
[46] R.M. Silverstein, F.X. Webster, Spectroscopic Identification of Organic Compound, 6th ed., John Willey & Sons, New York, 1998.
[47] A. Pawlukoj, J. Leciejewicz, Chem. Phys. 229 (2004) 39–45.
[48] G. Varsanyi, Assignments of Vibrational Spectra of Seven Hundred Benzene Derivatives, vols. 1–2, Adam Hilger, 1974.
[49] H.O. Kalinowski, S. Berger, S. Braun, Carbon-13 NMR spectroscopy, John Wiley & Sons, Chichester, 1988.
[50] K. Pihlaja, E. Kleinpeter (Eds.), Carbon-13 Chemical Shifts in Structural and Sterochemical Analysis, VCH Publishers, Deerfield Beach, 1994.
[51] F. Pretsch, P. Bühlman, C. Affolter, Structure Determination of Organic Compounds, Tables of Spectral Data, Springer-Verlag, Berlin, 2000.
[52] F.A. Cotton, C.W. Wilkinson, Advanced Inorganic Chemistry, 3rd ed., Interscience publisher, New York, 1972.
[53] D. Guillaumont, S. Nakamura, Dyes Pigments 46 (2000) 85–92.
[54] J. Fabian, Dyes Pigments 84 (2010) 36–53.
[55] L. Briquet, D.P. Vercauteren, J.M. André, E.A. Perpète, D. Jacquemin, Chem. Phys. Lett. 435 (2007) 257–262.
[56] Y. Ataly, D. Avci, A. BaSoglu, Struct. Chem. 19 (2008) 239–246.
[57] C. James, C. Ravikumar, T. Sundius, V. Krishnakumar, R. Kesavamoorthy, V.S. Jayakumar, I. Hubert Joe, Vib. Spectrosc. 47 (2008) 10–20.
[58] K. Fukui, Science 218 (1982) 747–754.